Journal of Chromatography, 186 (1979) 353–370

CHROM. 12,021

EARLY PHASES OF THE DISPERSION OF A SAMPLE INJECTED IN POISEUILLE FLOW

MARCEL J. E. GOLAY and JOHN G. ATWOOD
The Perkin-Elmer Corporation, Norwalk, Conn. 06856 (U.S.A.)

SUMMARY

A mathematical simulation of the dispersion of a sample injected in a viscosity-controlled (Poiseuille flow) stream has been made to determine the behavior of the sample from injection time until the sample distribution has become substantially gaussian. The results show that for velocities much greater than the chromatographic optimum, and for flow of the order one to ten theoretical plate heights, an unusually unsymmetrical distribution develops. It gives rise to doubly peaked chromatograms, in agreement with curves actually observed in corresponding experiments.

INTRODUCTION

When a miscible sample is injected uniformly in a cross-section of a viscous fluid carrier moving with Poiseuille flow within a round pipe, five phases can be distinguished in the dispersion of the sample within the carrier.

In a first phase the longitudinal dispersion will be due mainly to the static diffusion of the sample within the carrier. Designating by D the diffusion constant of the sample, its dispersion will be measured by the variance of its essentially gaussian distribution, which is given by:

$$\sigma_s^2 = 2Dt \tag{1}$$

where t refers to the time elapsed after injection and where the variance is with reference to an abscissa x measured along the pipe axis.

When carrier and sample are liquids, for which D is very small, of the order of 10^{-5} cm^2/sec or much less for large molecules, this first phase, during which the static diffusion given by eqn. 1 is dominant, will be brief, and will be succeeded by the second phase in which the variance of the sample spread is dominated by the effect of the carrier flow. The effect can be calculated as follows. Let the velocity v at any point at a distance r from the pipe axis be given by the expression:

$$v = 2v_0\left(1 - \frac{r^2}{r_0^2}\right) \tag{2}$$

where v_0 and r_0 designate the average carrier velocity and pipe radius, respectively. As we shall be concerned exclusively with the case in which the pipe inner wall is not coated by a retentive layer, v_0 will also be the average sample velocity. Were it not for the static diffusion measured by eqn. 1, the sample distribution with respect to x would assume the form of a box-car of length $2v_0t$. The variance of the box-car is:

$$\sigma_d^2 = \frac{(v_0t)^2}{3} \tag{3}$$

so that the total variance of the sample, given by the sum of the variances of the original static diffusion and of the Poiseuille flow spread, wou d be:

$$\sigma^2 = \sigma_s^2 + \sigma_d^2 = 2Dt + \frac{(v_0t)^2}{3} \tag{4}$$

However, as the components of the sample near the wall diffuse inward into the high velocity gradient of the flow near the wall, we enter a third phase in which the variance increases less rapidly than indicated by the right hand side of eqn. 4, as the rear-guard of the sample, which hugs the wall, catches up with the faster moving parts of the sample. Our study shows that the rear-guard forms a bump which rides on the rear of the boxcar and grows in width. In this third phase, because the velocity of the carrier near the pipe axis varies only quadratically with the distance r from this axis, the sample "front" near the axis is not seriously affected by diffusion into the slower portion of the carrier. This axial part of the front is affected only slightly by the small static diffusion in the x direction so that the leading edge of the box-car substantially retains its shape.

In the fourth phase, however, the central front has eventually lost its sharpness, and the rear-guard bump grows to consume the former box-car shape. The distribution has completely degenerated into a transitory shape which becomes more and more rounded. In the fifth phase, the sample distribution has again become a slightly skewed gaussian, and the rate of change of variance with time is:

$$\frac{d\sigma^2}{dt} = 2D_t \tag{5}$$

where D_t designates the total diffusion constant first calculated by Westhaver[1] and Taylor[2] and given by

$$D_t = D + \frac{r_0^2v_0^2}{48D} = D + D_d \tag{6}$$

where D_d designates the dynamic diffusion constant.

As no analytical treatment of fluid flow in pipe was available for the third and fourth phases identified above, it appeared worthwhile to make a computer-based determination of the several parameters such as variance, skewness, excess, etc. of the sample distribution during these phases, which is the subject of this paper.

MATHEMATICAL SIMULATION MODEL

In the model adopted, the sample within the pipe was considered to be distributed in 20 "tubes" within the pipe, the mth tube being the pipe portion comprised between two concentric cylinders at the distance $[(m-1)/20]\, r_0$ and $(m/20)\, r_0$ from the pipe center, with $m = 1, 2 \ldots 20$.

These 20 tubes were further divided into a suitable number of "rings of equal length and of different abscissa, all 20 rings of the same abscissa forming a "slice" within the pipe. The simulation consisted then of two alternating operations. The first was a forward "flow" operation in which sample in each tube was advanced according to its velocity. A small amount of lengthwise diffusion also took place. The second operation was an approximation of purely radial diffusion. Two such alternating operations are referred to as one "iteration".

At the outset the sample "injected" was divided into 400 parts, 1 part being injected in the first, or inner ring (actually a disc) of the injection slice, then 3 parts in the second ring, 5 in the third, etc., up to 39 parts in the 20th or outer ring. Since these numbers of parts are proportional to the volumes of the corresponding rings, an injection representing a uniform concentration of sample throughout the slice was achieved. As will be seen below, the total sample content of any one tube never varied.

In the flow operation which followed injection, and which simulated Poiseuille flow as closely as possible, the content of each ring was redistributed into three rings, generally in the forward (increasing x) direction in such a manner that the centroid of these three rings moved a whole or mostly fractional number of slices representative of an actual Poiseuille flow. Since this flow was given by eqn. 2, the flow for the mth ring was calculated as:

$$v = \frac{2\pi \int_{r_1}^{r_2} 2v_0 \left(1 - \frac{r^2}{r_0^2}\right) r \, dr}{2\pi \int_{r_1}^{r_2} r \, dr} = 2v_0 \left(1 - \frac{r_1^2 + r_2^2}{2r_0^2}\right) \tag{7}$$

or, computer-wise, since $r_1 = (m-1)\, r_0/20$ and $r_2 = m r_0/20$,

$$v = 2v_0 \left(1 - \frac{2m^2 - 2m + 1}{800}\right) \tag{8}$$

Thus, the flow was (799/400) v_0 for the sample content of the inner ring, (795/400) v_0 for the content of the second, etc. and (39/400) v_0 for the twentieth ring with v_0 designating the average number of slices by which the total sample content was translated forward in one iteration.

Let now $\Delta N + \varepsilon$ designate the number of slices by which the sample in any one given ring was translated forward, with ΔN an integer and $|\varepsilon| \leq 1/2$. The content in the ring was redistributed among the rings of the same tube $\Delta N - 1$, ΔN and $\Delta N + 1$ slices ahead, and these three rings were alloted the respective fractions $(1 - 2\varepsilon)^2/8$, $(3/4 - \varepsilon^2)$, and $(1 + 2\varepsilon)^2/8$ of the content of the ring thus moved, so that

the centroid of the three so-alloted portions was exactly $\Delta N + \varepsilon$ slices ahead, while the variance of this distribution, σ_1^2, is given by

$$\sigma_1^2 = \tfrac{1}{4}S^2 \tag{9}$$

where S is the physical length corresponding to one slice.

The radial diffusions within any one slice which alternate with the longitudinal flows are then obtained by redistributing the content of each ring as follows. One half the content of the inner ring ($m = 1$) is retained in it and the other half is placed in the second ring. The fraction 59/74 of the content of the outer ring ($m = 20$) is retained in it and the balance is placed in the nineteenth ring. As for any other mth ring, one half its content is retained while the fraction $(m - 1)/(4m - 2)$ is placed in the $(m - 1)$st ring and the fraction $m/(4m - 2)$ is placed in the $(m + 1)$st ring. The variance thus introduced by this redistribution is then one half of the square of the thickness of one ring. Normalizing the pipe radius to unity this variance is:

$$\sigma_2^2 = \frac{1}{2}\left(\frac{1}{20}\right)^2 = \frac{1}{800} \tag{10}$$

The two successive operations of translation forward and radial diffusion just described constitute one iteration, and are identically repeated for all rings and slices of the model several hundreds or even thousands of times to provide the insight sought in diffusive Poiseuille flow.

It will be noted that since the sample content injected into any two successive tubes m and $(m + 1)$ at the start are respectively proportional to $(2m - 1)$ and $(2m + 1)$ and since the radial diffusion causes the mth tube to deliver the fraction $m/(4m - 2)$ of its content to the $(m + 1)$st tube while receiving the fraction $m/(4m + 2)$ of the content of the latter, and since no interchanges take place between tubes during a translation the net interchange between any two consecutive tubes is always zero, and the content of each tube remains invariant for the entire simulation process. This parallels the physical model, in which there is no net radial motion of sample when summed over the whole length of the pipe.

Since the diffusive flow of any sample in a moving carrier is isotropic, the relationship between radial and longitudinal dimensions in the model should be such that the diffusion constant D should be equally valid radially and longitudinally. For the radial diffusion D is obtained from eqn. 1 in which we substitute its value from eqn. 10 for σ_2^2 and unity for the time of one iteration. This gives us:

$$\frac{1}{800} = 2D, \quad \text{or} \quad D = \frac{1}{1600} \tag{11}$$

But the same value of D must exist for the longitudinal diffusions which alternate with radial diffusion. Again setting $t = 1$ in eqn. 1 and using eqn. 9 we should have:

$$\tfrac{1}{4}S^2 = 2D = \frac{1}{800} \tag{12}$$

or

$$S = \frac{1}{\sqrt{200}} \tag{13}$$

i.e. the equivalent unit length longitudinally is $\sqrt{200} = 10\sqrt{2}$ slices.

The total diffusion D_t of eqn. 6 will be rewritten for the mathematical model thus:

$$D_t = \frac{1}{1600} + \frac{1600v_0^2}{48} \tag{14}$$

where the pipe radius r_0 has been given its normalized value unity. Likewise, the mathematical HETP h will be written:

$$h = \frac{2}{1600v_0} + \frac{1600v_0}{24} \tag{15}$$

and will be minimal (optimal) when both terms of the RHS are equal, *i.e.* for the chromatographic optimum velocity:

$$v_{opt}^2 = \frac{(2)(24)}{(1600)^2}$$

or:

$$v_{opt} = \frac{\sqrt{3}}{400} = 0.0043301 \text{ units/iteration}$$

and, with eqn. 13:

$$v_{opt} = \left(\frac{\sqrt{3}}{400}\right)(10\sqrt{2}) = 0.061237 \text{ slices/iteration} \tag{16}$$

which gives for h_{opt}:

$$h_{opt} = 2\frac{(2)(400)}{(1600)\sqrt{3}} = \frac{\sqrt{3}}{3} \text{ units} \tag{17}$$

or, with eqn. 13, $h_{opt} = 8.165$ slices.

RESULTS

Distribution of sample in the pipe

Figs. 1–5 show the simulated distribution of a sample in the pipe as a function of number of iterations T after a uniform injection into the slice at zero on the abscissa. Each figure is for one value of velocity ratio ranging from $v_0/v_{opt} = 1$ to $v_0/v_{opt} = 100$. For each distribution graph the abscissa scale is distance along the pipe expressed in theoretical plates at the corresponding velocity. The ordinate scale is sample content, expressed as percent of the slice having the maximum content. The curve marked "total" is the content of the whole slice. The curve marked "wall"

is the content of the 20th ring of each slice. The curve marked "center" is the content of the first ring, on the pipe axis. Because of its small volume, the sample content of this first ring is multiplied by 10 on all the graphs. As the sample peak moves down the pipe, these three curves preserve their mutual relationship, so they are

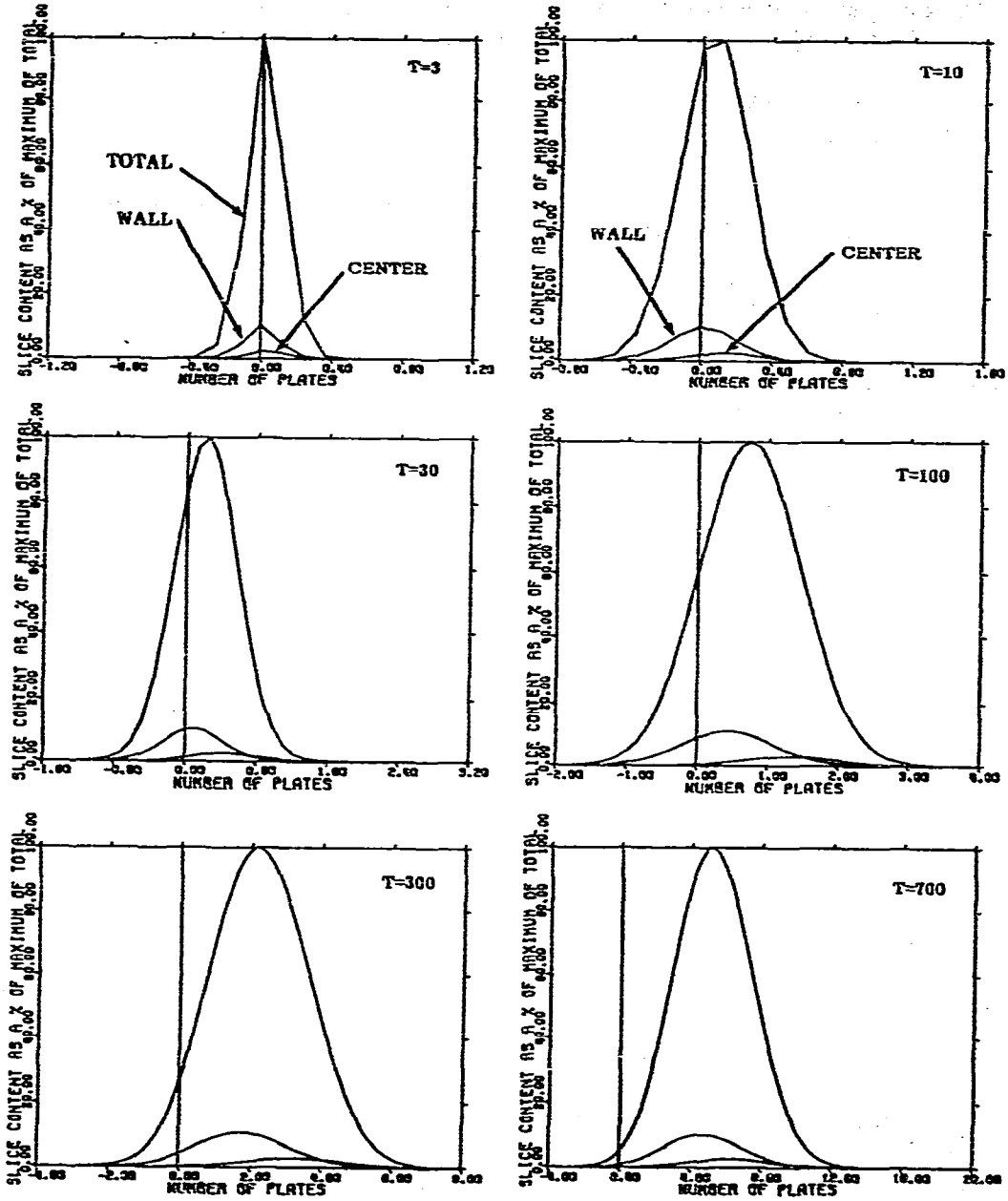

Fig. 1. Simulated sample distribution as a function of time T for $v_o/v_{opt} = 1$. T is expressed in iterations. Distance along the pipe is expressed in theoretical plates at this velocity. See text for explanation of curves.

marked in only the first graph of each figure. For the cases where $T = 3$ and 10, where the number of volume elements containing sample is very small, the distributions show oscillations or angularities which can be ignored as artifacts of the simulation model.

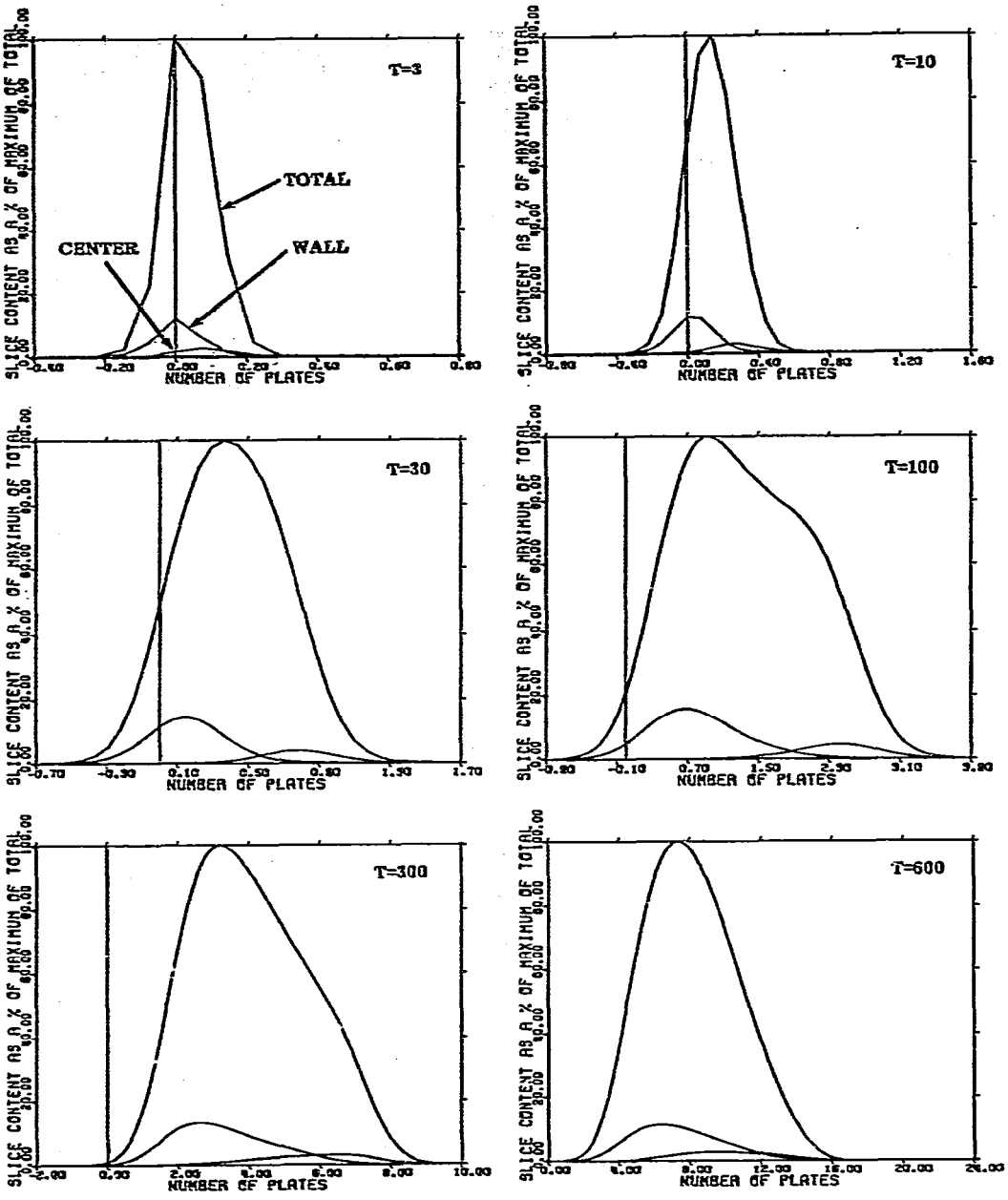

Fig. 2. Simulated sample distribution as a function of time T for $v_o/v_{opt} = 3$. T is expressed in iterations. Distance along the pipe is expressed in theoretical plates at this velocity. See text for explanation of curves.

For $v_0/v_{opt} = 1$, (and for all velocities smaller than this) the distributions always approximate a gaussian with varying degrees of skewness. The boxcar shapes and bumps of the second, third and fourth phases do not appear. This is shown in Fig. 1.

For $v_0/v_{opt} = 3$, the boxcar shapes of the second and third phases still do not

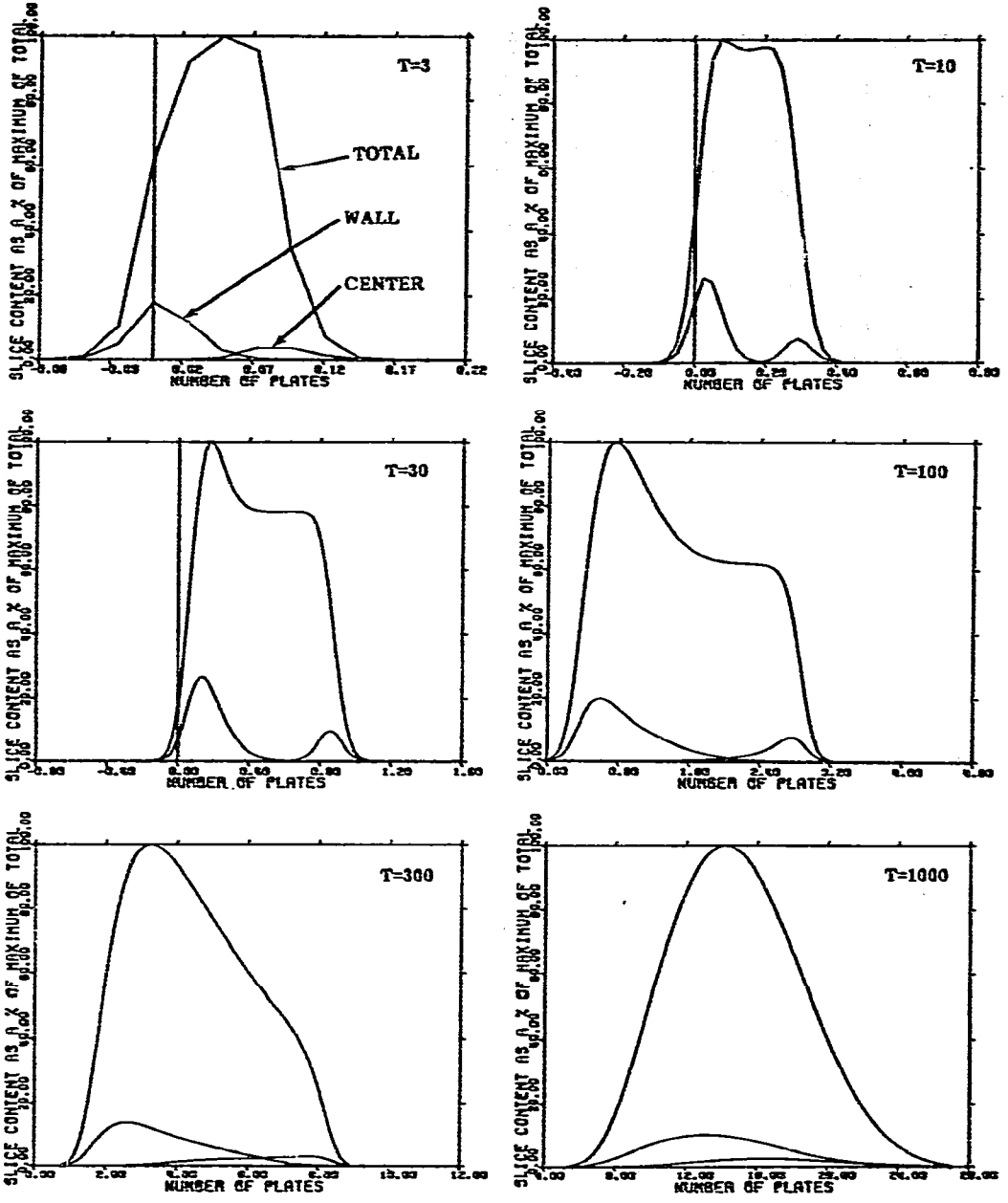

Fig. 3. Simulated sample distribution as a function of time T for $v_0/v_{opt} = 10$. T is expressed in iterations. Distance along the pipe is expressed in theoretical plates at this velocity. See text for explanation of curves.

appear, but at 100 iterations, the bumpy and strongly skewed shape of the fourth phase appears, and persists to about 600 iterations, where the moderately skewed gaussian of the fifth phase begins to appear. This is shown in Fig. 2.

For a velocity ratio $v_0/v_{opt} = 10$, where dynamic diffusion is 100 times more

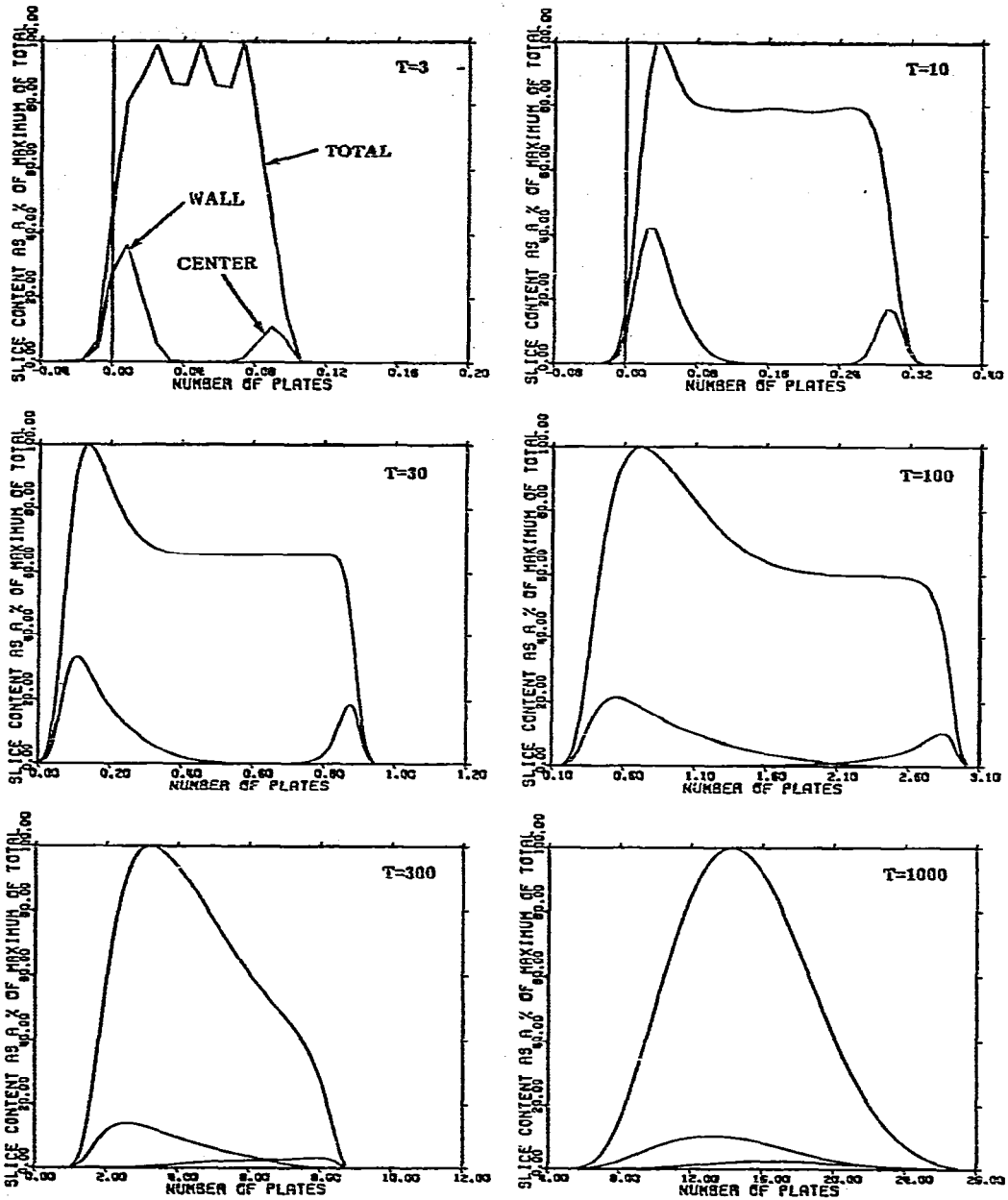

Fig. 4. Simulated sample distribution as a function of time T for $v_0/v_{opt} = 30$. T is expressed in iterations. Distance along the pipe is expressed in theoretical plates at this velocity. See text for explanation of curves.

significant than static diffusion the first gaussian phase is too brief to be resolved by the simulation method. From 10 to 30 iterations, the box-car shape develops. By 30 iterations it has a well formed rear-guard bump. By 300 iterations it is in the

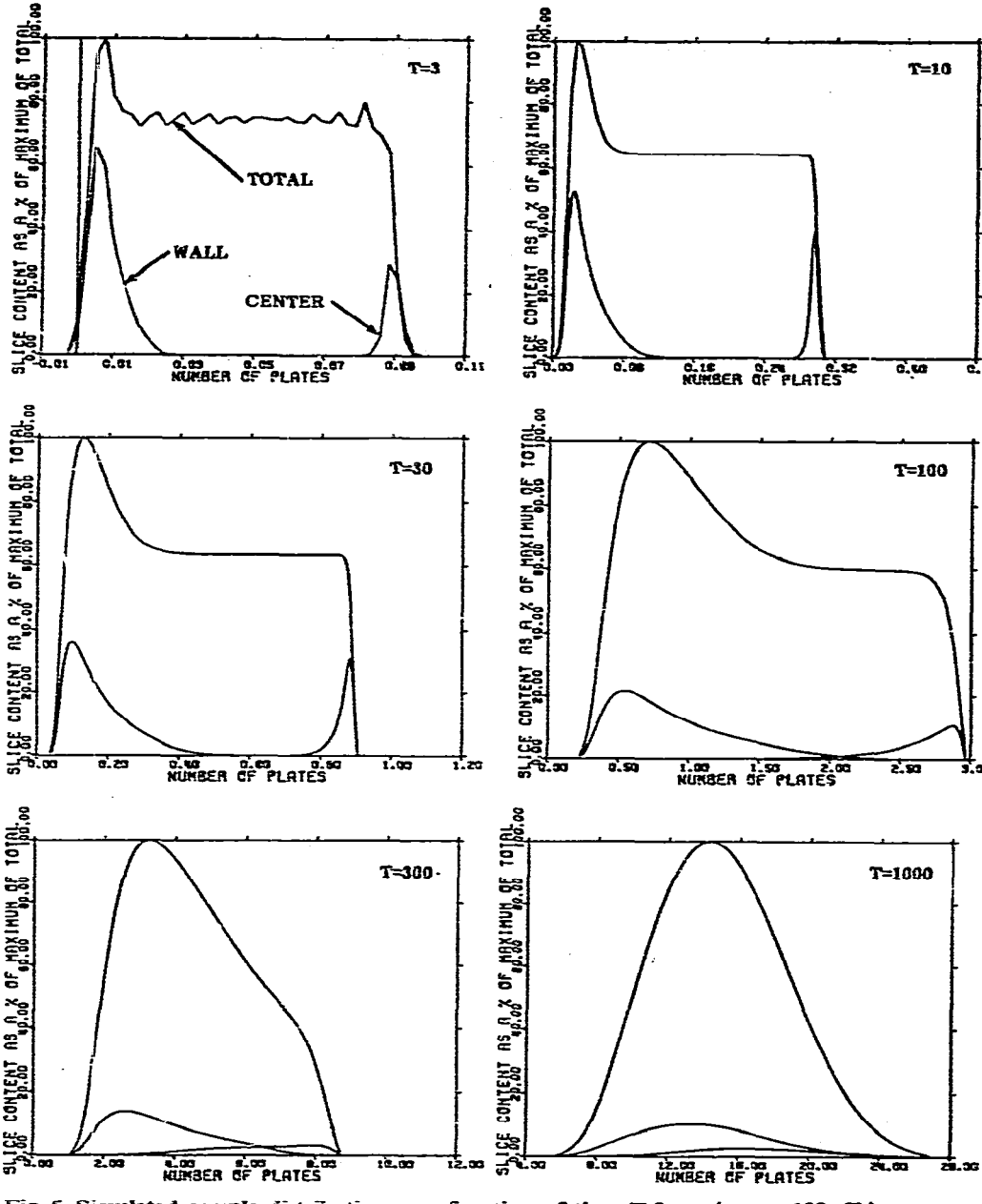

Fig. 5. Simulated sample distribution as a function of time T for $v_o/v_{opt} = 100$. T is expressed in iterations. Distance along the pipe is expressed in theoretical plates at this velocity. See text for explanation of curves.

strongly skewed fourth phase, and by 1000 iterations, the moderately skewed gaussian fifth phase has begun. These results are shown in Fig. 3.

When $v_0/v_{opt} = 30$ or greater, the flow is almost totally dominated by dynamic diffusion. The boxcar and the rear-guard bump develop very early and are well defined. The fifth phase starts after about 1000 iterations when the three inflection points on the leading edge merge into one.

It can be shown by analysis that after the sample has traveled more than about 10 theoretical plate heights, its distribution along any pipe radius becomes approximately gaussian, and that the distribution on the axis leads the distribution at the wall by the quantity:

$$e = \frac{v_0 r_0^2}{8D} \tag{18}$$

For $v_0/v_{opt} \gg 1$, this value of e is very nearly 3 plate heights. In the simulation results, Figs. 3, 4 and 5, for $v_0/v_{opt} = 10$, 30 and 100, respectively, show that the center distribution leads the wall distribution by about 3 plates, as expected.

Statistical properties of the distribution in the pipe

Figs. 6 and 7 confirm quantitatively that for v_0/v_{opt} of 30 or greater, the shapes of the distribution curves become virtually indistinguishable. Fig. 6 shows skewness versus iteration number for different values of v_0/v_{opt}. It measures the unsymmetrical departure from a gaussian shape. It shows that for high velocities all distributions reach a maximum skewness of about 0.34 at about 380 iterations. For high velocities, in the fifth phase at about 1000 iterations, the skewness approaches proportionality to $1/\sqrt{T}$. as expected by analogy with the behaviour of skewness in the one-dimensional case of the repeated convolutions of a simple distribution.

Fig. 7 shows the excess versus iteration number for different values of v_0/v_{opt}.

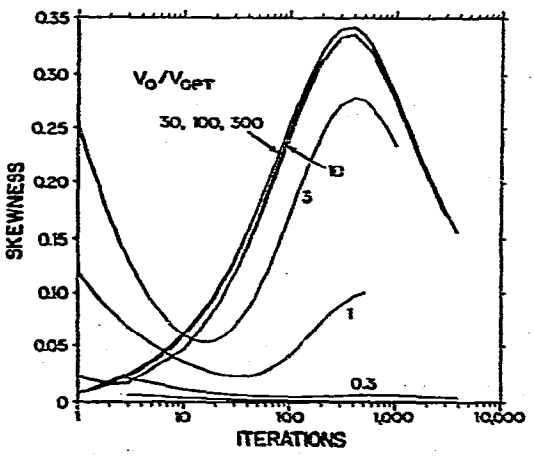

Fig. 6. Skewness of the simulated sample distribution as a function of time in iterations, with velocity ratio as a parameter. One theoretical plate is 66.67 iterations everywhere on the abscissa scale. Skewness is defined as (3rd moment)/(2nd moment)$^{3/2}$, where moments are about the mean.

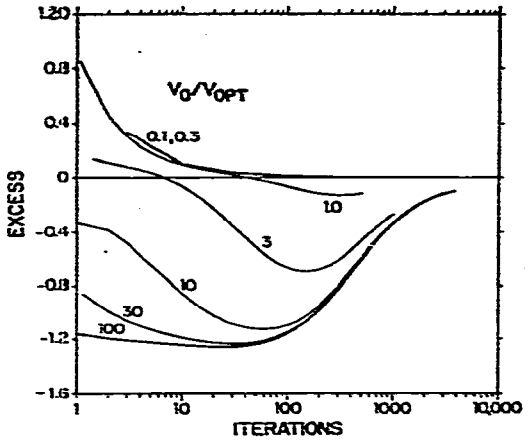

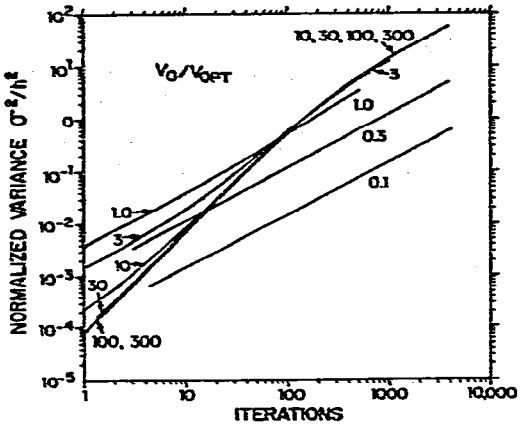

Fig. 7. Excess of the simulated distribution as a function of time in iterations with velocity ratio as a parameter. One theoretical plate is 66.67 iterations everywhere on the abscissa scale. Excess is defined as (4th moment)/(2nd moment)^2–3, where moments are about the mean.

Fig. 8. Normalized variance of the simulated sample distribution as a function of time in iterations, with velocity as a parameter. One theoretical plate is 66.67 iterations everywhere on the abscissa scale.

It measures the symmetrical departure from a gaussiar shape. The excess for a box-car shape is −1.20. As velocity increases the excess of the sample distributions approach this value earlier, and more closely until about 100 iterations. This reflects the dominance of the velocity gradient in producing the box-car shape in the second and third phases. Above 100 iterations, the excesses at velocity ratio 10 or greater rapidly converge with each other and pass through a maximum rate of change at about 380 iterations. They approach zero with proportionality to $1/T$. This is also as expected by analogy with the excess of repeated one-dimensional convolutions.

Behaviour of the variance

Fig. 8 shows the normalized variance of the total distribution in the pipe as a function of iterations, with velocity ratio as a parameter. Here, variance is expressed in units of theoretical plate height squared. It shows that for all velocities less than v_{opt}, variance is proportional to time, and increases with the square of velocity.

But for velocities much higher than v_{opt}, variance expressed in plate heights squared becomes independent of velocity ratio, increasing with the square of time below about 30 iterations, and proportional to time above about 1000 iterations.

Sample content of a given slice and elution of sample from pipe, as functions of time

Fig. 9 shows the simulated sample concentration as a function of time at six different fixed points along the pipe. The points chosen range from 0.1 to 30 theoretical plate heights downstream from the injection point. The velocity in the simulation was 100 times v_{opt}.

At each point two different ways of showing the concentration are presented. The curve marked "slice content" is the total sample content of the chosen slice as a function of iterations. Its physical counterpart is the measurement of concentration

in a sample cell forming an integral part of the flow path, *e.g.* the UV absorbance in a liquid chromatographic system with a flow cell which is a short segment of the connecting tubing.

The lower curve marked "elution" is the negative of the derivative with respect to time of the cumulative content of all slices upstream of the chosen slice. It represents the rate at which a sample would be eluted from the pipe if it ended at the chosen slice. Its physical counterpart is the signal from a detector that consumes the carrier fluid as it leaves the pipe and responds as a function of time to its average sample concentration. An example is a flame-ionization detector connected to a capillary gas chromatographic column.

Static diffusion generally causes some net backward flow of a sample as it disperses in Poiseuille flow, and the simulations for low velocity ratios show this as sample content upstream of the starting point in Figs. 1 and 2. But for velocity 100 times optimum, at a point 0.1 plates downstream from the start, it is completely negligible and does not occur in the simulation. For this reason all the elution curves look exactly the same as if the pipe ended at the chosen slice, even though the actual simulation was a single computation with the elution computed as the sample distribution passed each of the six chosen slices.

The slice content and elution curves are different because, while the slice content ignores the radial velocity gradient in the tube, the elution weights the flow at the center of the tube more heavily than the walls because the center is flowing faster. Since the sample distribution in the center of the tube always leads that at the walls, the elution curves always start, reach their peak, and decay earlier than the slice content curves. The shapes of the slice content curves are very different from the shapes of the sample distributions in the pipe because, especially for small numbers of plate heights, the distributions are changing very rapidly with time as they pass the points of measurement.

Nevertheless, the passage of the rear-guard bump on the box-car distribution can be seen in both slice content and elution curves. It produces a doubly peaked slice content curve most pronounced at about 3 plates.

Experimental observation of doubly peaked curves

For comparison with Fig. 9, Fig. 10 shows actual chromatograms produced by injecting a sample of sodium benzoate solution in a water mobile phase into a straight piece of stainless-steel tubing 366 cm long and 0.038 cm nominal I.D. An injection valve with a 6-μl loop was used. The detector measured UV absorbance in a flow cell with a volume of less than 3 μl. The system, without the 366-cm pipe removed had a bandwidth at half height of about 30 μl. Such a system could be expected to have a response between the slice content and elution curves, because there is some mixing of center and wall flows in the cell.

The length of the tube in theoretical plates was varied by varying the flow-rate as shown. The corresponding length in plates was estimated by computing the plates from the measured width at half height of the nearly gaussian curves obtained at flow-rates below 0.5 ml/min, and using the rule that plate height is proportional to flow-rate. This method avoids the need to know either the inside diameter of the tube or the diffusivity of the sample. Assuming the nominal diameter as correct,

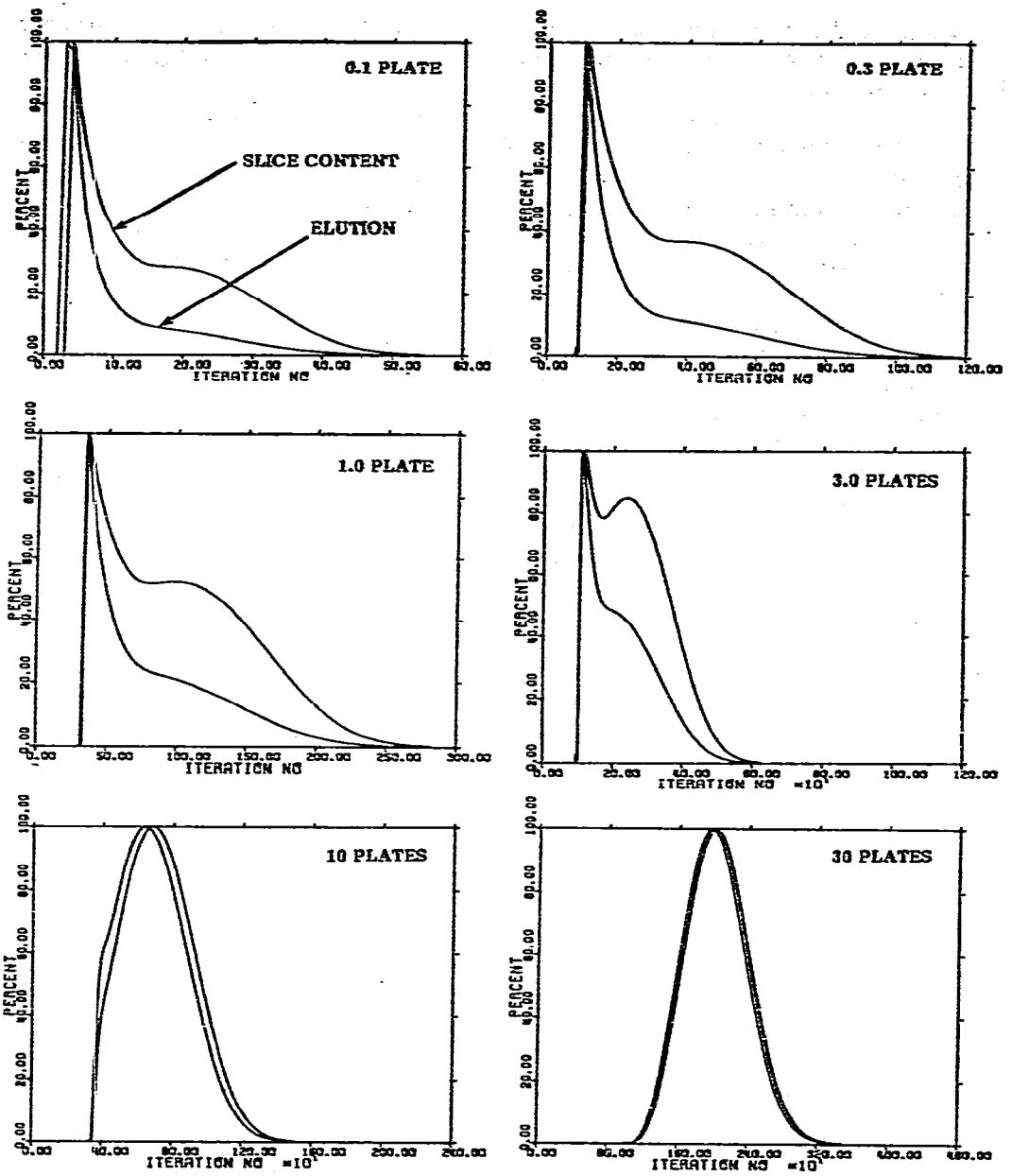

Fig. 9. Simulated slice content and elution curves versus time as a function of length of pipe for velocity ratio $v_o/v_{opt} = 100$. Length of pipe is expressed as theoretical plates at this velocity. Time is expressed as number of iterations. See text for explanation of curves.

then the corresponding diffusivity for sodium benzoate in water at room temperature was $8.3 \cdot 10^{-6}$ cm²/sec.

The progress of the bump on the experimental curves from 3.4 to 9.2 plates

resembles the shapes occurring over a somewhat wider range of plates in the simulated slice content curves. The expermental data, while quite repeatable, were also quite sensitive to straightness of the tube. The velocities in these experiments ranged from about 1000 v_{opt} to about 20,000 v_{opt}.

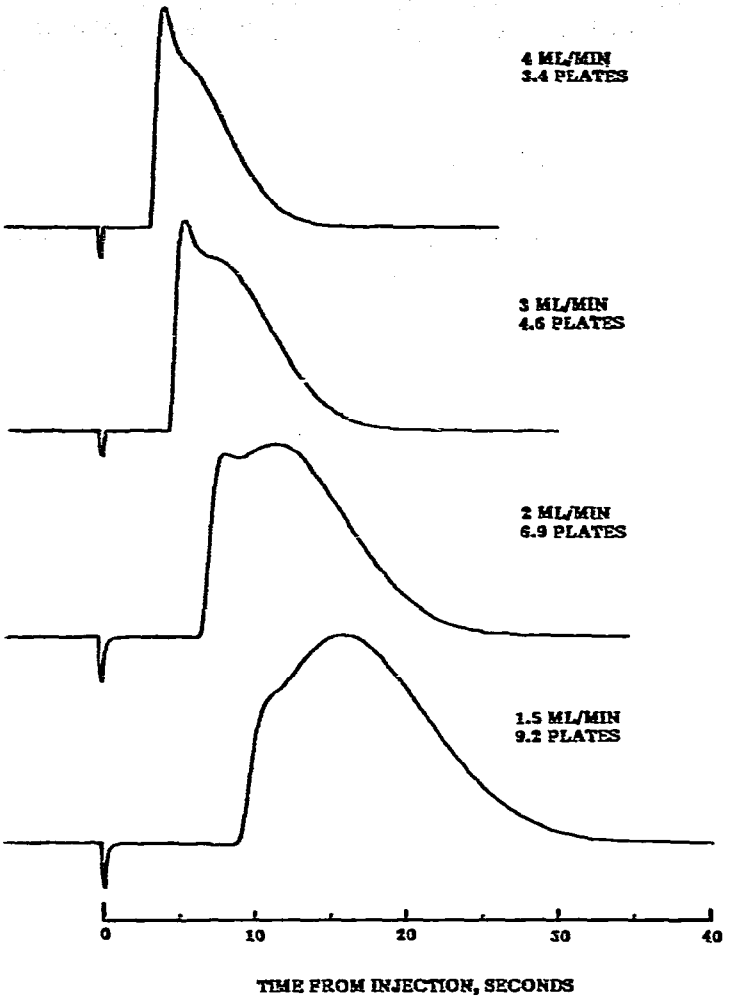

Fig. 10. Chromatograms produced by injecting sodium benzoate solution into a straight tube with 0.038 cm I.D. and length 366 cm. With this tube removed, the injection and detection system had a response to a 6-μl injection which had a width at half height of about 30 μl, and was delayed about 58 μl. See text for description.

DISCUSSION

Approximation for the total variance

In the pipes and flow cells of liquid chromatographic systems the velocities are typically thousands of times greater than v_{opt}. The effect of static diffusion is of the order of one millionth that of dynamic diffusion, and can be completely neglected.

The height of a theoretical plate is usually so large that the pipes are typically a fraction of a plate, or at most a few plates in length. Under these conditions we can use results from the simulation model to obtain a useful approximation of the variance contributed by these components.

The simulation results for $v_0 = 100\ v_{opt}$ are typical of all higher velocities. For short times after injection the variance due to the spreading box-car, from eqn. 3 is

$$\sigma_d^2 = \frac{(v_0 t)^2}{3} = \frac{\left(100\frac{\sqrt{6}}{40}T\right)}{3} = 12.5T^2\,(\text{slices})^2 \tag{19}$$

where T is the number of iterations. For very large T, we know the variance increases linearly with T, with coefficients calculated from eqn. 14:

$$\frac{d\sigma^2}{dT} = 2D_t = 2\left(\frac{1600v_0^2}{48}\right) = 2500\,(\text{slices})^2/\text{iteration} \tag{20}$$

We can approximate the total variance σ^2 over the whole range of T with a function that provides the correct square-law coefficient, A, for small T, and the correct slope, B for large T. This function is

$$\sigma_a^2 = \sqrt{(KB)^2 + B^2T^2} - KB \tag{21}$$

For $T \gg K$

$$\sigma_a^2 \cong AT^2 \tag{22}$$

while for $T \gg K$

$$\frac{d\sigma_a^2}{dT} \cong B \tag{23}$$

and the characteristic value of T which separates square law from linear dependency is:

$$K = \frac{B}{2A} \tag{24}$$

Thus $B = 2500$ (slices)^2/iteration, and $A = 12.5$ (slices)^2/(iteration)^2, with the result that $K = 100$ iterations. The approximated variance becomes:

$$\sigma_a^2 = \sqrt{250{,}000^2 + 12.5^2T^2} - 250{,}000 \tag{25}$$

Fig. 11 is a plot of σ_a/σ^2, where σ^2 is the total variance from the simulation model for $v_0 = 100\ v_{opt}$. The plot is asymptotic to 1 for high values of T. Below 2 iterations, it becomes slightly less than 1, reflecting the fact that the asymptote is

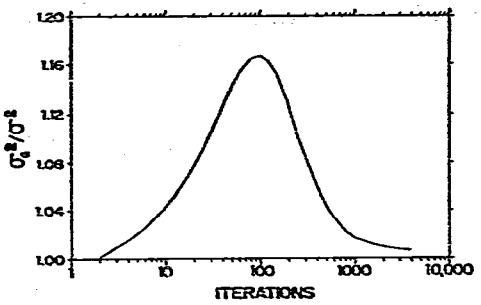

Fig. 11. Plot of the ratio σ_a^2/σ^2 as a function of time in iterations. One theoretical plate is 66.67 iterations everywhere on the abcissa scale. See text.

valid for very low times only when the velocity ratio approaches infinity. The plot has its greatest value of about 1.17 at $T = 100$ iterations.

That σ^2 is smaller than σ_a during the transition from box-car to gaussian distribution is attributed to the early forshortening of the tail end of the boxcar shape by diffusion in the high velocity gradient region.

Having learned the critical features of the distribution from this simulation, we can devise a generally applicable formula for its physical counterpart.

The number of plates, n represented by the characteristic time of 100 iterations in the simulation is:

$$n = 100\left(\frac{v_0}{h}\right) = 100\left(\frac{v_0}{\frac{1600 v_0}{24}}\right) = 1.5 \tag{26}$$

Therefore, in the physical counterpart time to flow 1.5 plates will also be the characteristic time. In the physical pipe, when $v_0 \gg v_{opt}$,

$$h = \frac{v_0 r_0^2}{24D}$$

The time, t_p, to flow one theoretical plate is

$$t_p = \frac{h}{v_0} = \frac{r_0^2}{24D} \tag{27}$$

so we can set the characteristic time in the formula

$$K = nt_p = 1.5\, t_p \tag{28}$$

We can now express the normalized variance for a box-car at times $t \gg 1.5\, t_p$ as

$$\frac{\sigma_d^2}{h^2} = \frac{\frac{(v_0 t)^2}{3}}{\left(\frac{v_0 r_0^2}{24D}\right)^2} = \frac{t^2}{3t_p^2} \tag{29}$$

Thus, in the approximate formula for normalized total variance, the coefficient A of the square law dependency is

$$A = \frac{1}{3t_p^2} \tag{30}$$

We can now use eqns. 24, 28 and 30 to find B.

$$B = 2AK = \frac{1}{t_p} \tag{31}$$

Substituting,

$$\frac{\sigma_s^2}{h^2} = \sqrt{(1.5)^2 + \frac{t^2}{t_p^2}} - 1.5 \tag{32}$$

If we define a function

$$\varphi(t/t_p) = \frac{\sigma_s^2}{\sigma^2}$$

we obtain the function plotted in Fig. 11.

Models of the early phases of distribution

A physical counterpart of the simulation described here is the spreading of an injected dye slug in a carrier travelling in a transparent tube. The quantitative observation of the nearly box-car distribution, with the more or less extended bump at its upstream portion, could be a worthwhile experiment.

ACKNOWLEDGEMENT

It is a pleasure to thank here Harold Jackson for the programming of the computer used for the simulation, and for several innovations in the presentation of results. Reference is made to him for any detailed information regarding the programs utilized.

REFERENCES

1 J. W. Westhaver, *J. Res. Nat. Bur. Stand.*, 38 (1947) 169.
2 G. Taylor, *Proc. Roy. Soc. A*, 255 (1956) 67.